# Interpreting the age dependency, diurnal variation, and pathological asymmetry of biophoton emission: an analytical hypothesis

Daqing Piao [1,2] PhD

[1] School of Electrical and Computer Engineering, Oklahoma State University, Stillwater, OK 74078, USA

[2] Department of Veterinary Clinical Sciences, Center for Veterinary Health Sciences, Oklahoma State University, Stillwater, OK 74078, USA

**Abstract:**

Biophoton emission has been experimented for decades. The photo-genic origin of biophoton has also been attributed to the oxidative stress or free radical production. However, there are considerable gaps in quantitative understanding of biophoton emission. In this work, I propose an analytical hypothesis for interpreting a few patterns of steady-state biophoton emission of human, including the dependency on age, the diurnal variation, and the geometric asymmetry associated with serious asymmetrical pathological conditions. The hypothesis is based on an alternative form of energy state, termed vivo-nergy, which is associated with only metabolically active organisms that are also under neuronal control. The hypothesis projects a decrease of the vivo-nergy in human during growth beyond puberty. The hypothesis also proposes a modification of the vivo-nergy by the phases of systematic or homeostatic physiology. The hypothesis further postulates that the deviation of the physiology-modified vivo-nergy from the pre-puberty level is deteriorated by acquired organ-specific pathological conditions. A temporal differential change of vivo-nergy is hypothesized to proportionally modulate oxidative stress that functions as the physical source of biophoton emission. The resulted steady-state diffusion of the photon emitted from a photo-genic source in a human geometry simplified as a homogeneous spherical domain is modeled by photon diffusion principles incorporating an extrapolated zero-boundary condition. The age and systematic physiology combined determines the intensity of the centered physiological steady-state photo-genic source. An acquired pathology sets both the intensity and the off-center position of the pathological steady-state photo-genic source. When the age-commemorated, physiology-commanded, and pathology-controlled modifications of the steady-state photo-genetic sources are implemented in the photon diffusion model, the photon fluence rate at the surface of the human-representing spherical domain reveals the patterns on age, the temporal variation corresponding to systematic physiology, and the geometric asymmetry associated with significant asymmetric pathological condition as reported for spontaneous biophoton emission. The hypothesis, as it provides conveniences for quantitative estimation of biophoton emission patterns, will be extended in future works towards interpreting the temporal characteristics of biophoton emission under stimulation.

**Keywords**: biophoton emission; age; temporal variation; asymmetry; analytical model; photon diffusion; steady-state.

Preprints (www.preprints.org) | NOT PEER-REVIEWED | Posted: 14 January 2019 doi:10.20944/preprints201810.0458.v2

## 1. Introduction

Spontaneous biophoton emission (Cifra and Pospisil, 2014) has been investigated over several decades under a variety of terms including the following that have appeared chronically: weak luminescence (Quickenden and Que Hee, 1974), low-level chemi-luminescence (Cadenas et al., 1980b), spontaneous chemi-luminescence (Boveris et al., 1984), biophoton(s) emission (Devaraj et al., 1997, Cohen and Popp, 1997), ultra-weak bioluminescence (Wang and Yu, 2009), auto-luminescence (Havaux et al., 2006), spontaneous ultra-weak light emission (Moraes et al., 2012), etc. The spectrum of biophoton emission interestingly covers the visible light and extends to ultraviolet and near-infrared bands (Cadenas et al., 1980b, Boveris et al., 1980, Cadenas, 1984, Gallas and Eisner, 1987, Devaraj et al., 1997, Kayatz et al., 2001, Kalaji et al., 2012, Fedorova et al., 2007, Zhao et al., 2017, Kobayashi et al., 2016, Wang et al., 2016). The commonly reported spontaneous biophoton emission intensity is several hundreds of photons per second per square centimeter (Cohen and Popp, 1997, Nakamura and Hiramatsu, 2005, Jung et al., 2005, Ou-Yang, 2014, Zhao et al., 2016). For a photon at the visible wavelength of 500nm, a photon count rate of 100 photons per second per square centimeter corresponds to an irradiance of $3.98 \times 10^{-17} W \cdot cm^{-2}$ or $\sim 0.04 fW \cdot cm^{-2}$. This irradiance is comparable to the photon fluence rate measured at 10cm from a source of 1μW power in an unbounded homogeneous tissue medium having an absorption coefficient of 0.106cm$^{-1}$ and a reduced scattering coefficient of 10cm$^{-1}$. The extremely small intensity makes spontaneous biophoton emission challenging to detect without completely darkened-out environment and highly sensitive photon detecting devices. The difficulty of detecting spontaneous biophoton emission also hinders the mechanism exploration beyond the known association of biophoton emission with the oxidative stress (Cadenas et al., 1980a) due to metabolic demands.

Although the photo-genic pathways of biophoton emission are less specified, the characteristics of biophoton regarding diffuse light emission are clearly inferred. A particularly robust observation of diffuse light emission properties of biophoton was made from human hand by Nakamura and Hiramatsu (Nakamura and Hiramatsu, 2005). In the presence of an air layer between the palm and the glass window of a photomultiplier tube (PMT), about 100 biophoton counts per second was obtained, while in the absence of air layer by the contact of PMT with the palm through mineral oil, about 200 biophoton counts per second was obtained. Similar level of biophoton counts was acquired by water-immerged contact of PMT with the palm or direct contact of the PMT glass window with the palm. The absence of air layer was justified as the sole attributer of the enhanced biophoton emission intensity. That observation supported the notion that the biophoton must have originated inside the skin. If biophoton originates inside the tissue, it will have to propagate within the tissue before evading the tissue at the boundary. A better matching of the refractive indices of the two media across the tissue boundary will thus reduce the loss of the photons crossing the boundary and consequently increase the biophoton emission intensity measured on the surface. The enhancement of biophoton emission by refractive index matching at the boundary converges to a boundary-value issue of light diffusion.

The variations of spontaneous biophoton emission intensity in association with normal physiological phases or environmental influences have been reported on different temporal scales. Diurnal rhythms of spontaneous biophoton emission of human have been linked to the systematic changes in energy metabolism inherent to a circadian cycle (Kobayashi et al., 2009). Frequency analysis of the spontaneous biophoton emission intensity revealed spectral components with longer-than-24-hours temporal characteristics ranging from 7-days to 270-days (Cohen and Popp, 1997, Cohen and Popp, 2003). Seasonal variation of spontaneous biophoton emission intensity (Jung et al., 2005, Zheng R, 1983, Cohen and Popp, 2003) revealed as high as 4-folds of changes over year-long measurements with the lowest intensity in the autumn and the highest intensity appearing 6-months apart from the autumn. The

spontaneous biophoton emission has also manifested gender and age-related variations (He et al., 2016, Sauermann et al., 1999, Yang W, 1996, Yang W, 1995, Zhao et al., 2016). The biophoton emission intensity was higher among males than among females, and higher in adults than in children. The aged male adult had ~40% higher biophoton emission intensity than the aged female adult (He et al., 2016). The biophoton emission of both male and female started to increase by the age of 11-14 and stabilize at ages around 50 (He et al., 2016). These findings indicate that measuring biophoton emission can potentially provide insight into the homeostatic state or systematic stage, as well as the harmonic correlation between the human body and the environment that is regarded fundamental to some alternative medical or healing practices (Sun et al., 2017). Deviations of the spontaneous biophoton emission intensity from these healthy temporal rhythms thus may render information of the deviation of the systematic or homeostatic physiological states from the normal levels.

The temporal variations of the human spontaneous biophoton emission intensity of normal physiological states also infer that, a human state departing significantly from healthy conditions due to acquired pathology may reveal a variation of biophoton emission intensity that is much stronger than that of a systematic cause. An acquired pathology that is site-specific could also cause the spontaneous biophoton emission pattern to be altered from a healthy balanced or symmetric configuration. An alteration of the biophoton emission by acquired pathology is likely the breaking of the symmetry of the spontaneous biophoton emission expected for a balanced faculty. A multiple sclerosis case was found to give ~200 biophoton counts/second in the right hand and ~300 biophoton counts/second in the left hand (Cohen and Popp, 1997). For hemiparesis patients, the hand of hemiparesis aspect emitted less biophotons in comparison to the contra-lateral normal hand (Jung et al., 2003), and acupuncture treatment reduced dramatically the left-right asymmetry of biophoton emission. The left-right asymmetry of spontaneous biophoton emission in a mouse model of human breast cancer (Zhao et al., 2017) became more pronounced as the tumor load in the right axillary increased versus the contra-lateral normal side. These reports suggest that the left-right asymmetry of spontaneous biophoton emission correlates with the left-right pathological differences.

The experimental observations have potentiated biophoton emission for non-invasive assessment of the health (Ives et al., 2014). The link between biophotons to the consciousness (Rahnama et al., 2011), mind-matter manipulation (Pederzoli et al., 2017, Joey M. Caswell, 2014), and paranormal phenomena at the moment of death (Reddy, 2016, St - Pierre, 2011) has also been suggested. However, there are considerable gaps in quantitative understanding of biophoton emission, in terms of interpreting some apparent patterns, even for the simplest steady-state cases. Model-based thus analytically-oriented interpretation of the spontaneous biophoton emission patterns could foster projection of the measurable patterns of stimulated biophoton emission that will be important for controlled experimental explorations to enhance targeted discovery of specific mechanisms underlying biophoton emission.

In this work, I propose an analytical framework of hypothesis for the initial objective of interpreting a few patterns of steady-state spontaneous biophoton emission of human, including the systematic dependency on age, the diurnal variation, and the geometric asymmetry associated with serious asymmetrical pathological conditions. The hypothesis assumes an alternative state of energy, termed “vivo-nergy,” which is associated with only metabolically active organisms that are also under neuronal control. The hypothesis projects a decrease of the vivo-nergy in human during growth beyond puberty, with the rate of decrease dictated by a time-constant set by the sexual maturity. The hypothesis also proposes a modification of the vivo-nergy by the phases of systematic or homeostatic physiology. The hypothesis further postulates that the deviation of the physiology-modified vivo-nergy from the pre-puberty level is deteriorated by the acquired organ-specific pathological conditions. The temporal differential change of vivo-nergy is hypothesized to be photo-genic, by proportionally modulating oxidative

Preprints (www.preprints.org) | NOT PEER-REVIEWED | Posted: 14 January 2019 doi:10.20944/preprints201810.0458.v2

stress that functions as the physical source of biophoton emission. The age and systematic physiology combined determines the intensity of the physiological photo-genic source that is simplified as centric to the body. An acquired pathology sets both the intensity and an off-center position of the pathological photo-genic source. The light emission from a photo-genic source will diffuse through the human body, which is simplified as a homogeneous translucent spherical domain. The photon diffusion through the body to the surface is modeled by photon diffusion principles incorporating an extrapolated zero-boundary condition. When the age-commemorated, physiology-commanded, and pathology-controlled modifications of the photo-genetic sources are implemented in the steady-state photon diffusion model, the steady-state photon fluence rate at the surface of the human-simplifying spherical domain can reveal the patterns of intensity dependence upon age, variation corresponding to systematic physiology, and geometric asymmetry associated with significant asymmetric pathological condition as reported in experimental spontaneous biophoton emission studies. The analytically-expressed hypothesis will be extended in future works to interpreting stimulated biophoton emission for the objective of characterizing the kinetics, which will be important for targeted experimental explorations of underlying mechanisms of biophoton emission in response to interventional or pathological stresses.

## 2. Analytical hypothesis of the photo-genic source of biophoton emission

A human life of natural course from birth to death can be regarded as experiencing three systematic changes: (1) the initial healthy increase and later matured stabilization of the body volume-contents, (2) the temporal variation of the biological phases by endocrine and exocrine controls, and (3) the deterioration of the body functions due to acquired pathological conditions. I hypothesize that a human body in the live state is associated with an alternative state of energy, named "vivo-nergy", which has a spatially and temporally resolved scalar energy density of $\mathbb{E}_{vivo}(\vec{\chi},t)$ (unit: $J\cdot s^{-1}\cdot cm^{-3}$) at a spatial position $\vec{\chi}$ and a time $t$. The scalar "vivo-nergy" $\mathbb{E}_{vivo}(\vec{\chi},t)$ takes the following form:

$$\mathbb{E}_{vivo}(\vec{\chi},t)=\mathbb{Z}_{prim}(\vec{\chi},t)\mathbb{H}_{syst}(\vec{\chi},t)\left[1-\mho_{path}(\vec{\chi},t)\cdot\mathbb{N}_{neuro}(\vec{\chi},t)\right], \quad (1)$$

where $\mathbb{Z}_{prim}(\vec{\chi},t)$ (unit: $W\cdot cm^{-3}$) denotes the "primo" state of "vivo-nergy" when inheriting from birth, $\mathbb{H}_{syst}(\vec{\chi},t)$ (unit: dimensionless) represents the phase of the systematic or homeostatic physiology that is endogenous to a healthy subject, $\mho_{path}(\vec{\chi},t)$ (unit: dimensionless) accounts for the effect of an acquired pathology that is exogenous to an otherwise healthy subject, and $\mathbb{N}_{neuro}(\vec{\chi},t)$ (unit: dimensionless) marks the neuronal networking to the site of the acquired pathology. Additionally, several absolute time-points or characteristic ages of the human life of natural course are symbolized as the following: $t_{birth}$ is the time of birth, $t_{death}$ is the time of death, $t_{puber}$ is the time of puberty so $\tau_{puber}=t_{puber}-t_{birth}$ is the age when puberty starts. At one's birth, the following initial conditions of the entities are inferred respectively: $\mathbb{Z}_{prim}(\vec{\chi},t_{birth})=\mathbb{Z}_0$, $\mathbb{H}_{syst}(\vec{\chi},t_{birth})=1$, $\mho_{path}(\vec{\chi},t_{birth})$=0, and $\mathbb{N}_{neuro}(\vec{\chi},t_{birth})=1$. The values of these parameters over the life-span of the person denoted by $t\in(t_{birth},t_{death}]$ is constrained respectively as the following: $\mathbb{Z}_{prim}(\vec{\chi},t)\in[0,\mathbb{Z}_0]$, $\mathbb{H}_{syst}(\vec{\chi},t)\in(0,1]$, $\mho_{path}(\vec{\chi},t)\in[0,1]$ and $\mathbb{N}_{neuro}(\vec{\chi},t)\in[0,1]$. A pathological condition that is terminal or lethal is represented by $\mho_{path}(\vec{\chi},t)=1$. A normal neuronal control of a site of pathological condition is marked by $\mathbb{N}_{neuro}(\vec{\chi},t)=1$. The complete loss of the neuronal control of a site of pathological condition is demarcated by $\mathbb{N}_{neuro}(\vec{\chi},t)=0$.

For a human life of normal course, it is also reasonable to assume that a life-shortening pathology is acquired after puberty, then the "primo" state of the vivo-nergy $\mathbb{Z}_{prim}(\vec{\chi},t)$ from birth to puberty would sustain at the initial level of $\mathbb{Z}_0$ set at birth with the only modification

Preprints (www.preprints.org) | NOT PEER-REVIEWED | Posted: 14 January 2019 doi:10.20944/preprints201810.0458.v2

incurring due to the systematic or homeostatic physiology $\mathbb{H}_{syst}(\vec{\chi},t)$. This results in a level-set representation of the vivo-nergy as the following, with the use of the Heaviside or unit step function $u(t)$:

$$\mathbb{E}_{vivo}(\vec{\chi},t) = \mathbb{Z}_0\left[u(t-t_{birth}) - u\left(t-t_{puber}\right)\right]\mathbb{H}_{syst}(\vec{\chi},t) + \mathbb{Z}_{adol}(\vec{\chi},t)\left[u\left(t-t_{puber}\right) - u(t-t_{death})\right]\mathbb{H}_{syst}(\vec{\chi},t)\left[1-\mho_{path}(\vec{\chi},t)\mathbb{N}_{neuro}(\vec{\chi},t)\right] \quad (2)$$

Where $\mathbb{Z}_{adol}(\vec{\chi},t)$ specifies the "primo" state of the energy counted from $t_{puber}$ as the person enters "adolescence", which decreases from the pre-puberty level as the following:

$$\mathbb{Z}_{adol}(\vec{\chi},t) = \mathbb{Z}_0\{1-\boxtimes(\vec{\chi},t)\} \quad (3)$$

where $\boxtimes(\vec{\chi},t) \leq 1$ is a non-negative value corresponding to the temporally resolved deficiency of $\mathbb{Z}_{adol}(\vec{\chi},t)$ from $\mathbb{Z}_0$. I define the temporal differential deviation of the vivo-nergy from the systematic physiology modified birth state of $\mathbb{Z}_0$ over the lifetime as the following:

$$\frac{\partial}{\partial t}[\Delta\mathbb{Z}_{vivo}(\vec{\chi},t)] = \frac{\partial}{\partial t}\left[\mathbb{Z}_0\mathbb{H}_{syst}(\vec{\chi},t) - \mathbb{E}_{vivo}(\vec{\chi},t)\right] \quad (4)$$

By using Eq. (2), it is straightforward to obtain the following:

$$\frac{\partial}{\partial t}[\Delta\mathbb{Z}_{vivo}(\vec{\chi},t)] = \langle\frac{\partial}{\partial t}\{[\mathbb{Z}_0 - \mathbb{Z}_{adol}(\vec{\chi},t)]\mathbb{H}_{syst}(\vec{\chi},t)\}\rangle\left[u\left(t-t_{puber}\right) - u(t-t_{death})\right] + \langle\frac{\partial}{\partial t}\{\mathbb{Z}_{adol}(\vec{\chi},t)\mathbb{H}_{syst}(\vec{\chi},t)\mho_{path}(\vec{\chi},t)\mathbb{N}_{neuro}(\vec{\chi},t)\}\rangle\left[u\left(t-t_{puber}\right) - u(t-t_{death})\right] \quad (5)$$

Two entities of differential properties are introduced as shown respectively in the following:

$$\frac{\partial}{\partial t}[\Delta\mathbb{Z}_{adol}(\vec{\chi},t)] = \mathbb{Z}_o\frac{\partial}{\partial t}\left[\boxtimes(\vec{\chi},t)\cdot\mathbb{H}_{syst}(\vec{\chi},t)\right] \quad (6)$$

$$\frac{\partial}{\partial t}\left[\Delta\mho_{path}(\vec{\chi},t)\right] = -\mathbb{Z}_0\frac{\partial}{\partial t}\left[\boxtimes(\vec{\chi},t)\cdot\mathbb{H}_{syst}(\vec{\chi},t)\mho_{path}(\vec{\chi},t)\mathbb{N}_{neuro}(\vec{\chi},t)\right] \quad (7)$$

Equation (5) then becomes

$$\frac{\partial}{\partial t}[\Delta\mathbb{Z}_{vivo}(\vec{\chi},t)] = \left\{\frac{\partial}{\partial t}[\Delta\mathbb{Z}_{adol}(\vec{\chi},t)] + \frac{\partial}{\partial t}\left[\Delta\mho_{path}(\vec{\chi},t)\right]\right\}\left[u\left(t-t_{puber}\right) - u(t-t_{death})\right] \quad (8)$$

where the first "differential" component associated with $\Delta\mathbb{Z}_{adol}$ as specified by Eq. (6) denotes the temporal deviation of the "vivo-nergy" from the "primo" state as a result of normal biological development, and the second "differential" component associated with $\Delta\mho_{path}$ as specified by Eq. (7) represents the further temporal deviation of the "vivo-nergy" from the level normal to an age due to acquired pathology.

The Eq. (8) by referring to Eqs. (6) and (7) will infer the age-dependency of the temporal differentiation of $\Delta\mathbb{E}_{vivo}$ by setting $\mathbb{H}_{syst}(\vec{\chi},t)$=1 and $\mho_{path}(\vec{\chi},t) = 0$, the effect of systematic physiology over a time period by setting $\mho_{path}(\vec{\chi},t) = 0$, and the outcome of acquired pathology at a given time point by setting $\mathbb{H}_{syst}(\vec{\chi},t)$=1. The hypothetic changes of the "vivo-nergy" over the life span of a human being are illustrated in **Figure 1**, where (A) marks the initial level of "vivo-nergy" set at birth, (B) specifies the decrease of "vivo-nergy" starting at puberty as a result of growth and aging, (C) represents the deviation of "vivo-nergy" from the age-related level due to modulation by systematic physiology, and (D) manifests the degradation of "vivo-nergy" from the healthy level for an age when caused by acquired pathology.

Preprints (www.preprints.org) | NOT PEER-REVIEWED | Posted: 14 January 2019 doi:10.20944/preprints201810.0458.v2

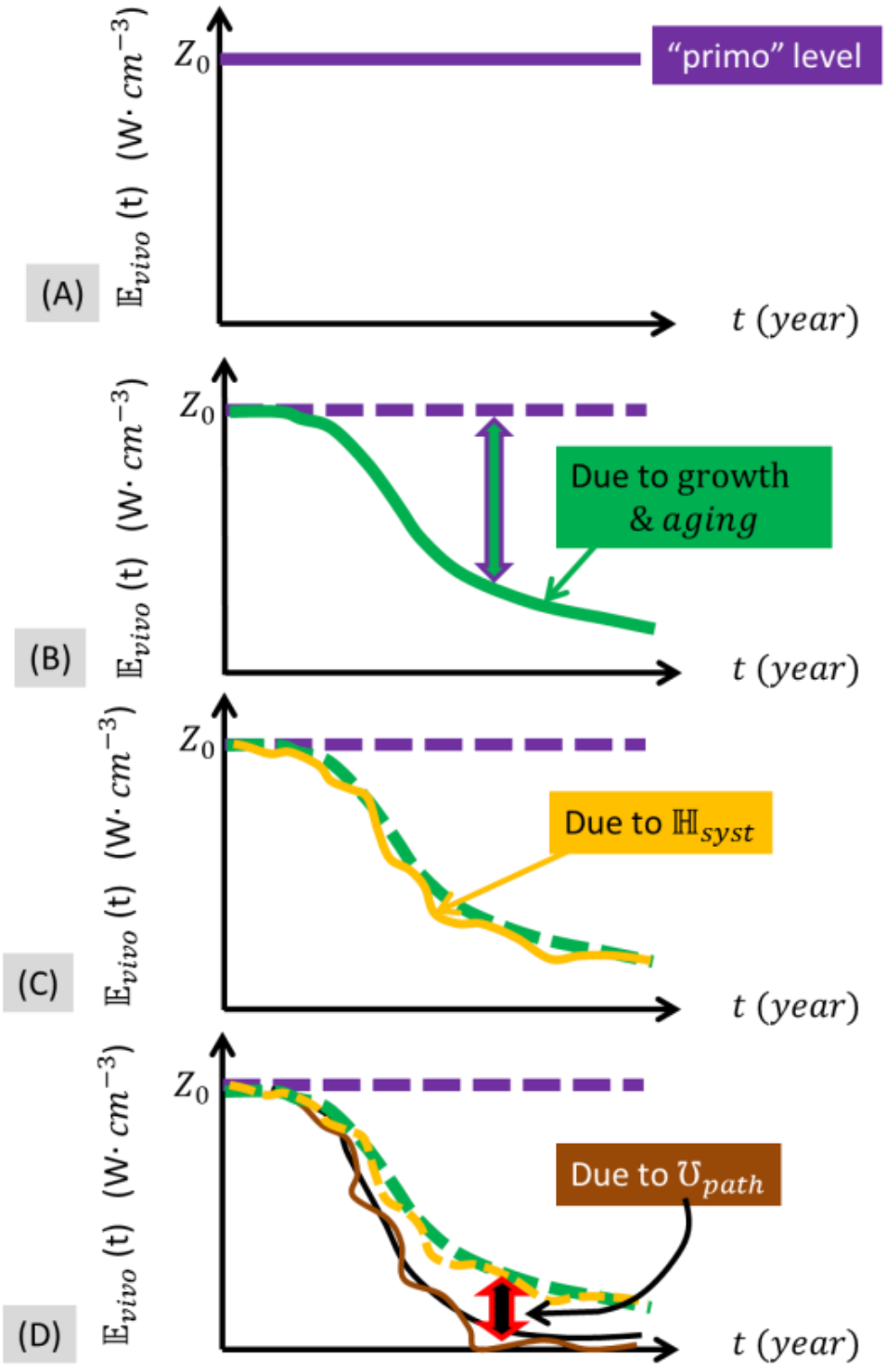


Figure 1. (A)The vivo-nergy bestowed on a person at birth. (B) The decrease of the "vivo-nergy" of a healthy person due to aging. (C) The modulation of the "vivo-nergy" of a healthy person by systematic physiology. (D) The degradation of the "vivo-nergy" of a person from the healthy level by acquired pathology.

Preprints (www.preprints.org) | NOT PEER-REVIEWED | Posted: 14 January 2019 doi:10.20944/preprints201810.0458.v2

I further hypothesize that the temporal differential change of the "vivo-nergy" is photo-genic through the oxidative bio-chemical pathways that produce free radicals (Slawinski et al., 1992, Burgos et al., 2016). So it is hypothesized that it is the changing rate of the "vivo-nergy" that modulates the oxidative stress. Integration of the spatially resolved temporal differentiation of the "vivo-nergy" gap represented by Eqs. (6) and (7) over the body volume gives rise to the following two spectrally and temporally resolved photo-genic intensity terms:

$$\mathbb{S}_{syst}(\lambda,t) = \varrho_{syst}(\lambda,t) \iiint \frac{\partial}{\partial t}[\Delta\mathbb{Z}_{adol}(\vec{\chi},t)]\, d\vec{\chi}^3 \tag{9}$$

$$\mathbb{S}_{path}(\lambda,t) = \eth_{path}(\lambda,t) \iiint \frac{\partial}{\partial t}\left[\Delta\mho_{path}(\vec{\chi},t)\right] d\vec{\chi}^3 \tag{10}$$

where $\varrho_{syst}(\lambda,t)$ (unit: dimensionless) is the spectrally and temporally resolved physiological-photogenic factor, and $\eth_{path}(\lambda,t)$ (unit: dimensionless) is the spectrally and temporally resolved pathological-photogenic factor. The human body for the initial simplicity is treated as a volume of spherical domain of radius $R_0$ as shown in **Figure 2**. The physiological photo-genic source $\mathbb{S}_{syst}$ (unit: W) is set at the center of the spherical domain, whereas the pathological photo-genic source $\mathbb{S}_{path}$ (unit: W) that may be associated with a single serious organ-specific pathology could be positioned at any distance $\mathrm{R}_{path}$ to the center. The spherical coordinates of the pathological photo-genic source $\mathbb{S}_{path}$ are set as $(\mathrm{R}_{path},\theta',\phi')$, or for convenience of visualization at the 3 o'clock position with respect to the center of the spherical body. The spectral and temporal dependences of the photo-genic sources $\mathbb{S}_{syst}$ and $\mathbb{S}_{path}$ are not considered in the following, i.e. $\varrho_{syst}(\lambda,t) = \varrho_{syst} = constant$, $\eth_{path}(\lambda,t) = \eth_{path} = constant$, thus $\mathbb{S}_{syst}$ and $\mathbb{S}_{path}$ are steady-state sources that will facilitate analysis of the simplest steady-state photon propagation in the body volume.

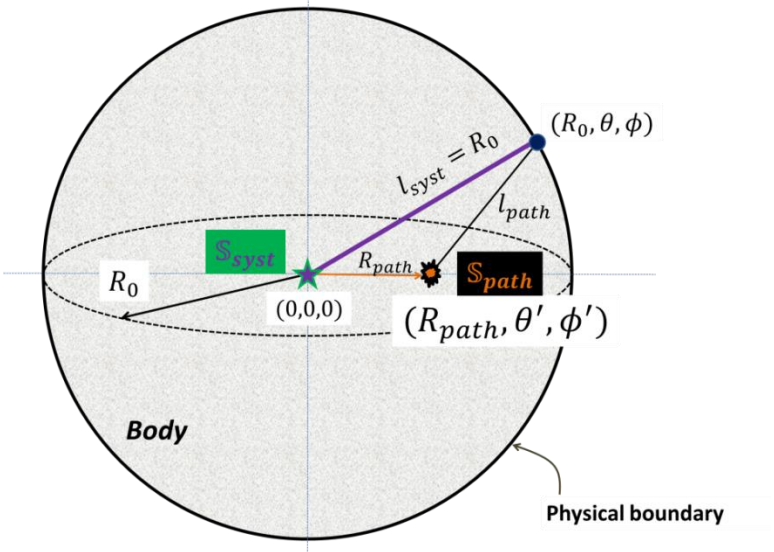


Figure 2. The human body is simplified as a spherical geometry with a radius $R_0$. The physiological photo-genic source $\mathbb{S}_{syst}$ is set at the center of the spherical domain, or with the spherical coordinates of (0,0,0). The pathological photo-genetic source $\mathbb{S}_{path}$ is positioned at 3 o'clock position with respect to the spherical center, at $(\mathrm{R}_{path},0,0)$. The distance of any position $(\mathrm{R}_0,\theta,\phi)$ on or off the spherical surface to the pathological source $\mathbb{S}_{path}$ is denoted as $l_{path}$.

Preprints (www.preprints.org) | NOT PEER-REVIEWED | Posted: 14 January 2019 doi:10.20944/preprints201810.0458.v2

## 3. Steady-state photon diffusion causing surface photon emission

With the placement of a steady-state photo-genic source in the spherical tissue domain representing the human body, the steady-state propagation of the photon in the spherical domain that is several orders greater than the photon scattering path-length in a biological tissue can be readily modeled by the diffusion approximation to the radiative transfer equation (Ishimaru, 1989). The human body is treated in the present work as a globally homogeneous diffusive medium containing localized steady-state spatially impulsive photo-genic sources. The diffusive tissue medium is characterized by the following properties: absorption coefficient $\boldsymbol{\mu_a}$ [unit: cm$^{-1}$], reduced scattering coefficient $\boldsymbol{\mu_s'}$ [unit: cm$^{-1}$], diffusion coefficient $\boldsymbol{D = 1/[3(\mu_a + \mu_s')]}$ [unit: cm], and effective attenuation coefficient $\boldsymbol{\mu_{eff} = \sqrt{\mu_a/D}} = \sqrt{\boldsymbol{3\mu_a\mu_s'}}$ [unit: cm$^{-1}$]. For a field or detection position at $\vec{\chi} = (r, \theta, \varphi)$ within the globally homogeneous tissue domain including that on the tissue-air boundary, the steady-state photon fluence rate $\boldsymbol{\Psi(\vec{\chi})}$ (unit: s$^{-1}$cm$^{-2}$) satisfies the following governing equation (Contini et al., 1997):

$$\nabla^2\Psi(\vec{\chi}) - \frac{\mu_a}{D}\Psi(\vec{\chi}) = -\frac{S(\vec{\chi})}{D} \tag{11}$$

where $S(\vec{\chi})$ is a source term, which is also subject to a boundary condition as all boundary-involved electromagnetic problems are. For an infinite homogeneous medium containing a steady-state point source at $\vec{\chi}'$ with an intensity $S$ as is represented by $S \cdot \delta(\vec{\chi}')$, Eq. (11) has the well-known Green's function solution of (Zhang et al., 2010)

$$\Psi(\vec{\chi}, \vec{\chi}') = \frac{S}{4\pi D}\frac{1}{|\vec{\chi} - \vec{\chi}'|}exp\left(-\mu_{eff}|\vec{\chi} - \vec{\chi}'|\right) \tag{12}$$

The solution Eq. (12) can also be written in the following Eigen function expansion (Piao et al., 2015):

$$\Psi(\vec{\chi}, \vec{\chi}') = \frac{S}{D}\left(\mu_{eff}\right)\sum_{l=0}^{\infty}\left[i_l\left(\mu_{eff}r_<\right)\cdot k_l\left(\mu_{eff}r_>\right)\right]\sum_{m=-l}^{l}[Y_{lm}^*(\theta', \phi')\cdot Y_{lm}(\theta, \phi)] \tag{13}$$

where $i_l$ and $k_l$ are respectively the $l$-th order modified spherical Bessel function of the first and the second kinds, $r_<$ and $r_>$ are respectively the smaller and greater radial coordinates between the source and the detector, and $Y_{lm}$ is the spherical harmonics function.

With regards to the effect on photon fluence rate by the tissue-air boundary, it has been established that the photon fluence rate does not become zero at a field position immediately beyond the tissue boundary; instead, a more accurate treatment of extrapolated zero-boundary condition sets zero the photon fluence rate at a distance away from the tissue boundary-------the so called extrapolated zero-boundary (Haskell et al., 1994). The Figure 2 with the implementation of the extrapolated zero-boundary is illustrated in **Figure 3**. A field point $\vec{\chi}$ on or beyond the spherical tissue boundary locates at $(r, \theta, \varphi)$ with $r \geq R_0$. The application of the extrapolated zero-boundary condition to the photon fluence rate associated with any source within the tissue medium is satisfied by introducing an "image" of the source with respect to the extrapolated zero-boundary that is co-centric with and at a radial distance of $R_b = 2AD$ outward from the physical boundary (Piao et al., 2015) where $A = (1 + \xi)/(1 - \xi)$, $\xi = -1.440n^{-2} + 0.710n^{-1} + 0.668 + 0.0636n$, and $n$ is the refractive index of the air-bounding tissue. As the composite photon fluence rate resulted from both the physical source in the tissue medium and the image of it becomes zero at the extrapolated zero-boundary, the composite positive photon fluence rate elsewhere resulted from the same two sources of one being physical and the other being imaginary thus become the solution in the associated physical space within the body volume or beyond the boundary, according to the uniqueness characteristics of all electromagnetic properties.

Preprints (www.preprints.org) | NOT PEER-REVIEWED | Posted: 14 January 2019 doi:10.20944/preprints201810.0458.v2

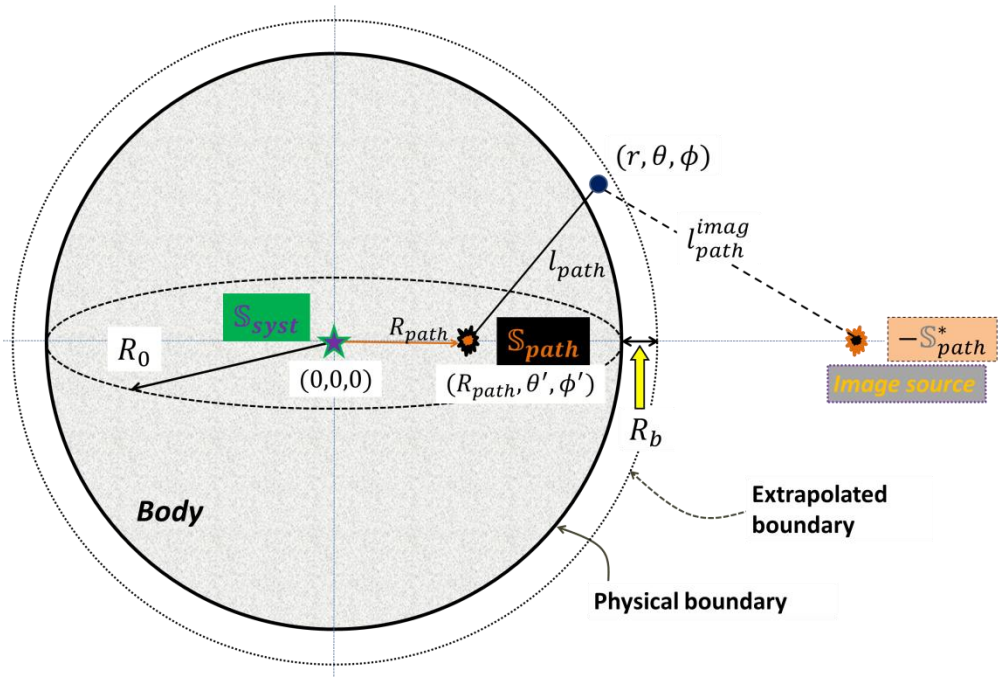


Figure 3. The human body containing a physiological photo-genic source of $\mathbb{S}_{syst}$ at the center of the spherical domain, and a single pathological photo-genetic source $\mathbb{S}_{path}$ at $(\mathrm{R}_{path},0,0)$. The photon emitted by a photo-genic source diffuses in the human body and encounters a refractive index discontinuity at the body boundary. The effect of the tissue-air boundary is accounted for by setting the photon fluence rate at an imaginary boundary extrapolated from the physical boundary at a distance of $\mathrm{R}_b$. The image of the single pathological photo-genetic source $\mathbb{S}_{path}$ locates at the radial direction of $\mathbb{S}_{path}$ due to the obvious symmetry. The intensity of the image of the single pathological photo-genetic source $\mathbb{S}_{path}$ may become - $\mathbb{S}_{path}$ in the case of the tissue becoming semi-infinite domain.

For the pathological photo-genic source $\mathbb{S}_{path}$ located off-center at $(R_{path},\theta',\phi')$, the geometric symmetry determines that the image of it with respect to the extrapolated zero-boundary must locate along the same radial direction of it. The source $\mathbb{S}_{path}$ and its image with respect to the extrapolated zero-boundary thus collectively set zero the photon fluence rate on the extrapolated zero-boundary. Based on Eq. (13), the photon fluence rate associated with the pathological photo-genic source $\mathbb{S}_{path}$ and evaluating on the extrapolated zero-boundary, for which the source locates at $r_< = R_{path}$ and the field point locates at $r_> = R_0 + R_b$, is

$$\Psi_{path}\big|_{extra} = \mathbb{S}_{path}\frac{1}{D}(\mu_{eff})\sum_{l=0}^{\infty} i_l[\mu_{eff}\cdot(R_{path})]\cdot k_l[\mu_{eff}(R_0+R_b)]$$
$$\sum_{m=-l}^{l} Y_{lm}^{*}(\theta',\phi')Y_{lm}(\theta,\phi) \qquad (14)$$

where the notation "$_{left}\big|_{right}$" indicates evaluating the "left" as the source on the "right" as the field position. Note that any "$l$"th order (or moment) of the pathological photo-genic source has the same intensity of $\mathbb{S}_{path}$. Similarly, the photon fluence rate associated with the image of the pathological photo-genic source and evaluating on the extrapolated zero-boundary, for which

Preprints (www.preprints.org) | NOT PEER-REVIEWED | Posted: 14 January 2019 doi:10.20944/preprints201810.0458.v2

the source now locates at a radial position of a to-be-determined $r_>$ and the detector locates at $r_< = R_0 + R_b$, is

$$\Psi_{path}^{imag}\big|_{extra} = \frac{1}{D}(\mu_{eff})\sum_{l=0}^{\infty} S_l^* \cdot i_l[\mu_{eff}(R_0 + R_b)] \cdot k_l[\mu_{eff} r_>] \sum_{m=-l}^{l} Y_{lm}^*(\theta', \phi') Y_{lm}(\theta, \phi) \quad (15)$$

where the $S_l^*$ terms is different for different "$l$" (or moment). Based on the essence of "image-source" (Piao et al., 2015, Zhang et al., 2010), the two unknown terms $S_l^*$ and $r_>$ associated with the $l$-th order (or moment) "image" source (the $k_l$ component) can be expressed by a single unknown term $S_l$ associated with the same order (or moment) of the actual pathological photo-genic source $\mathbb{S}_{path}$ located within the tissue at $(R_{path}, \theta', \phi')$ (the $i_l$ component), as the following:

$$S_l^* \cdot k_l[\mu_{eff} r_>] = S_l \cdot i_l[\mu_{eff}(R_{path})] \quad (16)$$

Applying the extrapolated zero-boundary condition of $\Psi_{path}\big|_{extra} + \Psi_{path}^{imag}\big|_{extra} = 0$ leads to

$$S_l = -\mathbb{S}_{path} \frac{k_l[\mu_{eff}(R_0+R_b)]}{i_l[\mu_{eff}(R_0+R_b)]} \quad l = 0,1,2,\ldots \quad (17)$$

Now for the photon fluence rate associated with the pathological photo-genic source at $(R_{path}, \theta', \phi')$, but evaluating at a field point between the body boundary and the extrapolated zero-boundary, the source still locates at $r_< = R_{path}$ but the detector or the field point locates at $r_> = R_0 + \Delta r$, where $\Delta r \in [0, R_b]$. For the photon fluence rate associated with the image of the pathological photo-genetic source and also evaluating at a field point between the body boundary and the extrapolated zero-boundary, the field point now locates at $r_< = R_0 + \Delta r$ and the source terms are known through Eqs. (16) and (17). Collectively the composite photon fluence rate originating from a pathological photo-genic source at $(R_{path}, \theta', \phi')$ and sensed by a detector or field point at $(R_0 + \Delta r\,, \theta, \phi)$ between the body boundary and the extrapolated zero-boundary becomes:

$$\begin{aligned}
\Psi_{path} &= \Psi_{path}\big|_{field} + \Psi_{path}^{imag}\big|_{field} \\
&= \frac{\mathbb{S}_{path}}{D}(\mu_{eff})\sum_{l=0}^{\infty} i_l[\mu_{eff}(R_{path})] \cdot k_l[\mu_{eff}(R_0 + \Delta r)] \sum_{m=-l}^{l} Y_{lm}^*(\theta', \phi') Y_{lm}(\theta, \phi) \\
&- \frac{\mathbb{S}_{path}}{D}(\mu_{eff})\sum_{l=0}^{\infty} \cdot i_l[\mu_{eff}(R_0 + \Delta r)] i_l[\mu_{eff}(R_{path})] \cdot \frac{k_l[\mu_{eff}(R_0 + R_b)]}{i_l[\mu_{eff}(R_0 + R_b)]} \sum_{m=-l}^{l} Y_{lm}^*(\theta', \phi') Y_{lm}(\theta, \phi) \\
&= \frac{\mathbb{S}_{path}}{D}(\mu_{eff})\sum_{l=0}^{\infty} i_l[\mu_{eff}(R_{path})] \cdot k_l[\mu_{eff}(R_0 + \Delta r)] \sum_{m=-l}^{l} Y_{lm}^*(\theta', \phi') Y_{lm}(\theta, \phi) \\
&\quad \left\{1 - \frac{i_l[\mu_{eff}(R_0+\Delta r)]}{k_l[\mu_{eff}(R_0+\Delta r)]} \frac{k_l[\mu_{eff}(R_0+R_b)]}{i_l[\mu_{eff}(R_0+R_b)]}\right\}
\end{aligned} \quad (18)$$

Equation (18) contains two parts: the "1" in the bracket represents the infinite-medium contribution to the photon fluence rate by the pathological photo-genic source $\mathbb{S}_{path}$ that can be expressed by the simple form of Eq. (12); and the other term in the bracket scales the infinite-medium contribution to the photon fluence rate by the image of the pathological photo-genic

Preprints (www.preprints.org) | NOT PEER-REVIEWED | Posted: 14 January 2019 doi:10.20944/preprints201810.0458.v2

source $\mathbb{S}_{path}$ with respect to the former one. By using some analytics of the modified spherical Bessel function and Eq. (12), Eq. (18) is converted to the following form (Piao et al., 2015)

$$\Psi_{path} = \frac{\mathbb{S}_{path}}{4\pi D}\frac{1}{l_{path}} exp\left(-\mu_{eff} l_{path}\right)\left\{1 - \frac{I_{l+1/2}[\mu_{eff}(R_0+\Delta r)]}{K_{l+1/2}[\mu_{eff}(R_0+\Delta r)]}\frac{K_{l+1/2}[\mu_{eff}(R_0+R_b)]}{I_{l+1/2}[\mu_{eff}(R_0+R_b)]}\right\} \quad (19)$$

where $I_{l+\frac{1}{2}}$ and $K_{l+\frac{1}{2}}$ are respectively the $\left(l+\frac{1}{2}\right)$-th order modified Bessel function of the first and the second kinds. For a human body simplified as a spherical domain, it is easy to have an $R_0$ (i.e., 10cm) that is substantially greater than 10 times of $1/\mu_{eff}$ to have the second term in the bracket of Eq. (19) approximated by

$$\frac{I_{l+1/2}[\mu_{eff}(R_0+\Delta r)]}{K_{l+1/2}[\mu_{eff}(R_0+\Delta r)]}\frac{K_{l+1/2}[\mu_{eff}(R_0+R_b)]}{I_{l+1/2}[\mu_{eff}(R_0+R_b)]} = exp\left[-2\mu_{eff}(R_b-\Delta r)\right] \quad (20)$$

Thus Eq. (19) will be changed to a trivial form of

$$\Psi_{path} = \frac{\mathbb{S}_{path}}{4\pi D}\frac{1}{l_{path}} exp\left(-\mu_{eff} l_{path}\right)\left\{1 - exp\left[-2\mu_{eff}(R_b-\Delta r)\right]\right\} \quad (21)$$

Equation (21) that is associated with the pathological photo-genic source of $\mathbb{S}_{path}$ conveniently satisfies the condition of producing zero composite photon fluence rate at the extrapolated zero-boundary whereupon $\Delta r = R_b$. Equation (21) also determines that the photon fluence rate associated with the pathological photo-genic source of $\mathbb{S}_{path}$ decreases monotonically from the body boundary to the extrapolated zero-boundary. One can find that, a hypothetical movement of the photo-genic source like the pathological one $\mathbb{S}_{path}$ from $(R_{path}, \theta', \phi')$ toward the center of the spherical domain can maintain the boundary-resulted composite photon fluence rate as the form of Eq. (21), with the length dimension $l_{path}$ varying according to the position of the photo-genic source. The hypothetical experiment infers that the boundary-resulted composite photon fluence rate at a field point at $(R_0 + \Delta r, \theta, \varphi)$ in association with a physiological photo-genic source $\mathbb{S}_{syst}$ located at the center of the spherical domain can be represented as the following:

$$\Psi_{syst} = \frac{\mathbb{S}_{syst}}{4\pi D}\frac{1}{l_{syst}} exp\left(-\mu_{eff} l_{syst}\right)\left\{1 - exp\left[-2\mu_{eff}(R_b-\Delta r)\right]\right\} \quad (22)$$

where $l_{syst}$ is the distance from the physiological photo-genic source to the field point. When both the physiological patho-genic source $\mathbb{S}_{syst}$ and the pathological photo-genic source $\mathbb{S}_{path}$ are considered as the origins of the photon emission causing photon distribution beyond the spherical boundary, the composite photon fluence rate at a field point $(R_0 + \Delta r, \theta, \varphi)$ is thus the combination of the respective photon flounce rates of Eqs. (21) and (22), as the following:

$$\Psi_{total} = \frac{1}{4\pi D}\left[\mathbb{S}_{syst}\frac{1}{l_{syst}} exp\left(-\mu_{eff} l_{syst}\right) + \mathbb{S}_{path}\frac{1}{l_{path}} exp\left(-\mu_{eff} l_{path}\right)\right] \left\{1 - exp\left[-2\mu_{eff}(R_b-\Delta r)\right]\right\} \quad (23)$$

Preprints (www.preprints.org) | NOT PEER-REVIEWED | Posted: 14 January 2019 doi:10.20944/preprints201810.0458.v2

## 4. Numerical evaluation of the superficial photon fluence rate over the spherical domain

Equation (23) can be implemented numerically to assess the patterns of steady-state photon fluence rate presenting at or beyond the air-interfacing boundary of the human-representing spherical homogeneous tissue domain, in association with the physiological photo-genic source $\mathbb{S}_{syst}$ alone or the addition of the pathological photo-genic source $\mathbb{S}_{path}$. The distribution of the steady-state photon fluence rate across the surface of the human-representing spherical domain and expanding to the extrapolated zero-boundary is exemplified in **Figure 4**. The tissue medium used for all numerical evaluations in this section is specified with the following dimensional and optical properties: a radius of $R_0 = 10cm$, an absorption coefficient of $\mu_a = 0.1\ \text{cm}^{-1}$, a reduced scattering coefficient of $\mu_s' = 10\ \text{cm}^{-1}$, and a refractive index of n=1.4. The tissue optical properties result in a distance of $R_b = 0.11cm$ of the extrapolated zero-boundary from the tissue boundary, which is only 1.1% of the radius of the spherical domain. When the tissue medium represented by the spherical domain contains only the centered physiological photo-genic source $\mathbb{S}_{syst}$, the photon fluence rate on the entire spherical boundary has to be uniform, and the photon fluence rate will decrease from the tissue boundary to become zero at the extrapolated zero-boundary. The degradation of the steady-state photon fluence rate from the tissue boundary to the extrapolated zero-boundary over an entire azimuthal or elevational circle will appear as a thin circular strip of 0.11cm thick around the spherical tissue domain. To better visualize this thin circular strip of the steady-state photon fluence rate around the spherical tissue domain in Figure 4, the evaluation of the Eq. (23) over the space beyond the tissue boundary is conducted over a radial distance of 10 times of $R_b$, i.e. a 1.1cm distance from the tissue boundary as the strip of lower color value outside the dashed circle demarcating the spherical tissue boundary. In obtaining Fig. 4, the following additional parameters are necessary: $\mathbb{S}_{syst} = 0.01\mu W$ and $\mathbb{S}_{path} = 0$. The uniform photon fluence rate across the spherical tissue domain represents the 2-dimentional projection of the photon fluence rate measured on the surface of the spherical tissue domain as is the case for measurement/imaging using a planar pixelated photon detection device. The steady-state photon fluence rate projected on the surface of a spherical tissue domain of the associated optical properties with a 10cm radius and a 0.01μW source at the center is at the level of $1\times 10^{-17} W\cdot cm^{-2}$ (corresponding to 25 counts of 500nm photons per second per $\text{cm}^2$), and drops to zero at the extrapolated zero-boundary that in actual scale is just about 0.11cm or 1.1mm away from the tissue boundary of the specified optical properties.

In the following sections, the numerical implementations of Eq. (23) are configured in 3 cases of the photo-genetic sources to demonstrate the possibility of revealing respectively the most apparent superficial patterns of age-dependency, physiological variation, and pathological asymmetry of the steady-state photon-fluence rate at the surface of the spherical domain. It is noted that the macroscopic temporal variation is assessed via relative changes of the steady-state photon fluence rate evaluated at the same spatial location over a macroscopic time-scale that is many orders longer than the time of light propagation in the tissue domain. Therefore when the steady-state photon fluence rate is to be evaluated at one position to assess the temporal changes at any macroscopic durations, the position of the field point is set at the spherical tissue boundary and at the 3 o'clock position, and the resulted steady-state photon fluence rate is normalized for comparing against a few literature data of spontaneous steady-state biophoton emission that are reproduced with the copyrighters' permissions.

Preprints (www.preprints.org) | NOT PEER-REVIEWED | Posted: 14 January 2019 doi:10.20944/preprints201810.0458.v2

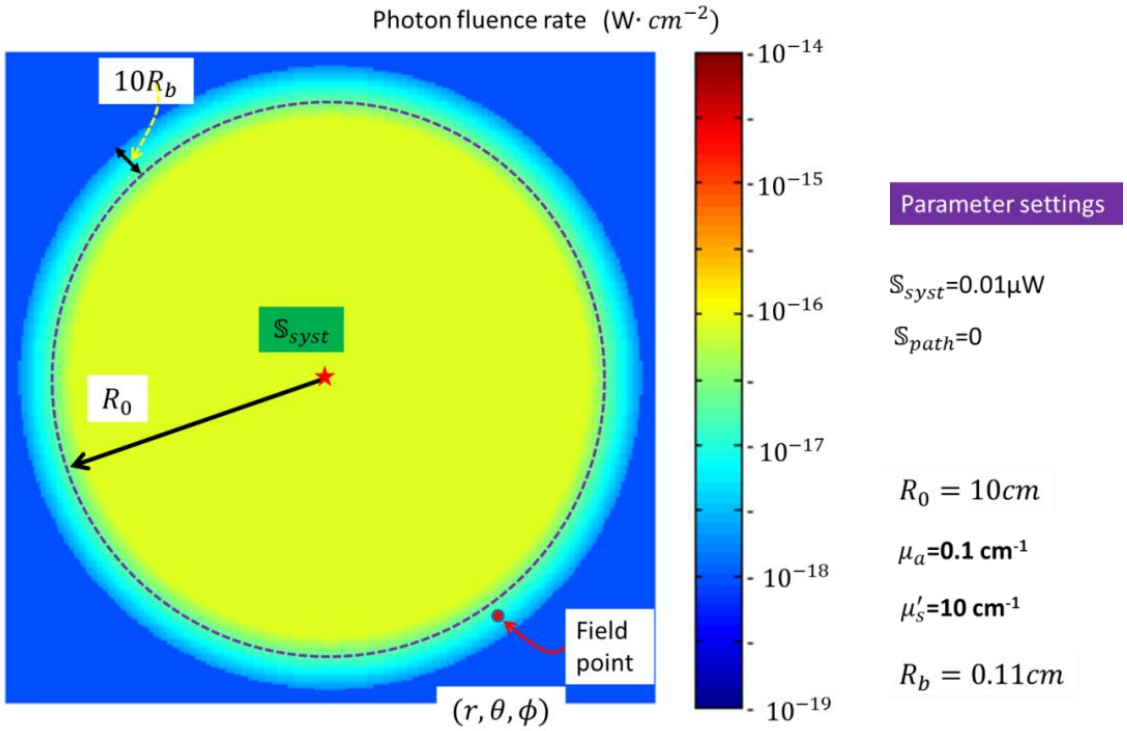


Figure 4. Example of the distribution of the photon fluence rate across the surface of the human-representing spherical domain and expanding to the extrapolated boundary. The degradation of the photon fluence rate from the tissue boundary to the extrapolated boundary over an entire azimuthal or elevational circle illustrates as a thin circular strip around the spherical tissue domain.

### 4.1 Presentation of the age dependency

In order to simulate the age dependency, it is necessary to hypothesize the age-dependent physiological photo-genesis. I define $\tau_{fossi}$ as the age of a person's first opposite-sex sexual intercourse (FOSSI). A person who commits heterosexual activities at least once in lifetime will have $t_{birth} < t_{puber} < (t_{birth} + \tau_{fossi}) < t_{death}$. A person who remains virgin in lifetime will have $\tau_{fossi} = (t_{death} - t_{birth})$. I define the systematic photo-genesis of biophoton emission as a result of aging to take the following form

$$\mathbb{S}_{syst}(\lambda, t) = \left[1 - exp\left(-\frac{t - t_{puber}}{\tau_{fossi}}\right)\right]^{\alpha} \quad (24)$$

where $\alpha$ is a positive number or an ageing factor. The age dependency and gender difference of the photon fluence rate at the boundary of the spherical tissue domain is simulated by removing $\mathbb{S}_{path}$ and setting the following parameters: the puberty age $\tau_{puber}$ of male is 13, the puberty age $\tau_{puber}$ of female is 11, the FOSSI age $\tau_{fossi}$ of both male and female is 20, the ageing factor is $\alpha = 2$, and a life spans 75 years. The male tissue density is assumed to be greater than the female at the same age, leading to stronger intensity of the physiological photo-genic source $\mathbb{S}_{syst}$ for male than female at otherwise identical setting of the parameters. Alternatively, stronger adipose contents of female could cause a higher scattering attenuation of the photon

Preprints (www.preprints.org) | NOT PEER-REVIEWED | Posted: 14 January 2019 doi:10.20944/preprints201810.0458.v2

propagation to result in lesser photon emission at the surface of the body under the same physical dimensions. A literature report showing the dependency of spontaneous biophoton counts on age and the difference of biophoton counts between male and female is reproduced with permission from the publisher (He et al., 2016) as shown in **Figure 5**(A). In (A) there is a smaller down-ward solid-framed arrow pointing to an age group of 11-14 of both male and female, at which the biophoton count started to increase noticeably. That age group is projected to indicate puberty. In (A) there is a larger upward dash-framed arrow pointing to an age group of 41-50 of the female that may be interpreted for menopause. That menopause-inferring change is not included in the numerical model analysis *per se*. The numerical results as specified heretofore are plotted in Figure 5(B) with the assumption that the photon fluence rate has a baseline count at the level of the literature report.

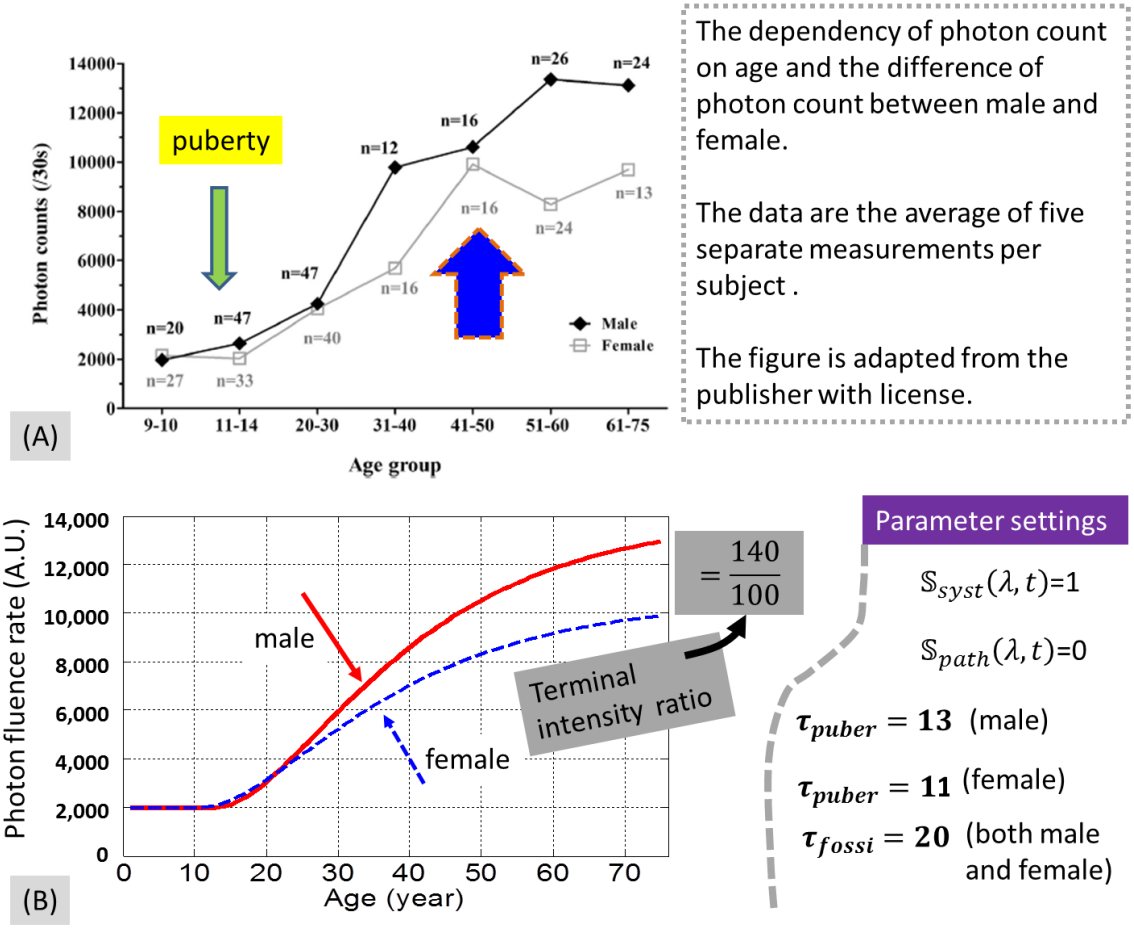


Figure 5. The age dependency and gender difference of the biophoton emission demonstrated in a literature study (He et al., 2016) in (A) and the simulated photon fluence rate at the boundary of the spherical tissue domain in (B). (A) There is a smaller down-ward solid-framed arrow pointing to an age group of 11-14 of both male and female, at which the spontaneous biophoton count started to increase noticeably. That age group is projected to indicate puberty. In (A) there is a larger upward dash-framed arrow pointing to an age group of 41-50 of the female that may be interpreted as indicating menopause.

Preprints (www.preprints.org) | NOT PEER-REVIEWED | Posted: 14 January 2019 doi:10.20944/preprints201810.0458.v2

### 4.2 Presentation of the diurnal variation

The variation of the photon fluence rate revealed at the boundary of the spherical tissue domain as a function of short-term homeostatic changes is simulated by removing $\mathbb{S}_{path}$ and setting the $\mathbb{H}_{syst}$ and thus $\mathbb{S}_{syst}(\lambda, t)$ to change periodically. A known diurnal variation of the spontaneous biophoton count is adopted from an open-access publication (CIFRA M, 2007) as shown in **Figure 6**(A). The spontaneous biophoton emission intensity revealed a trough in the later afternoon and a peak in early morning. That diurnal variation over a range of approximately 90-110% of the mid-line level can be directly attributed to the circadian cycle. The circadian cycle is thus implemented into the intensity of physiological photo-genic source in Eq. (23) by setting $\mathbb{S}_{syst}(\lambda, t) = 0.9 + 0.1cos\left(\frac{\pi}{4}t - \frac{\pi}{2}\right)$. This circadian-like systematic change results in $\mathbb{S}_{syst}(\lambda, t)$ to vary between 1 and 0.8. The resulted photon fluence rate as shown in (b) varies at a cycle close to that manifested by the more noisy presentation of (A).

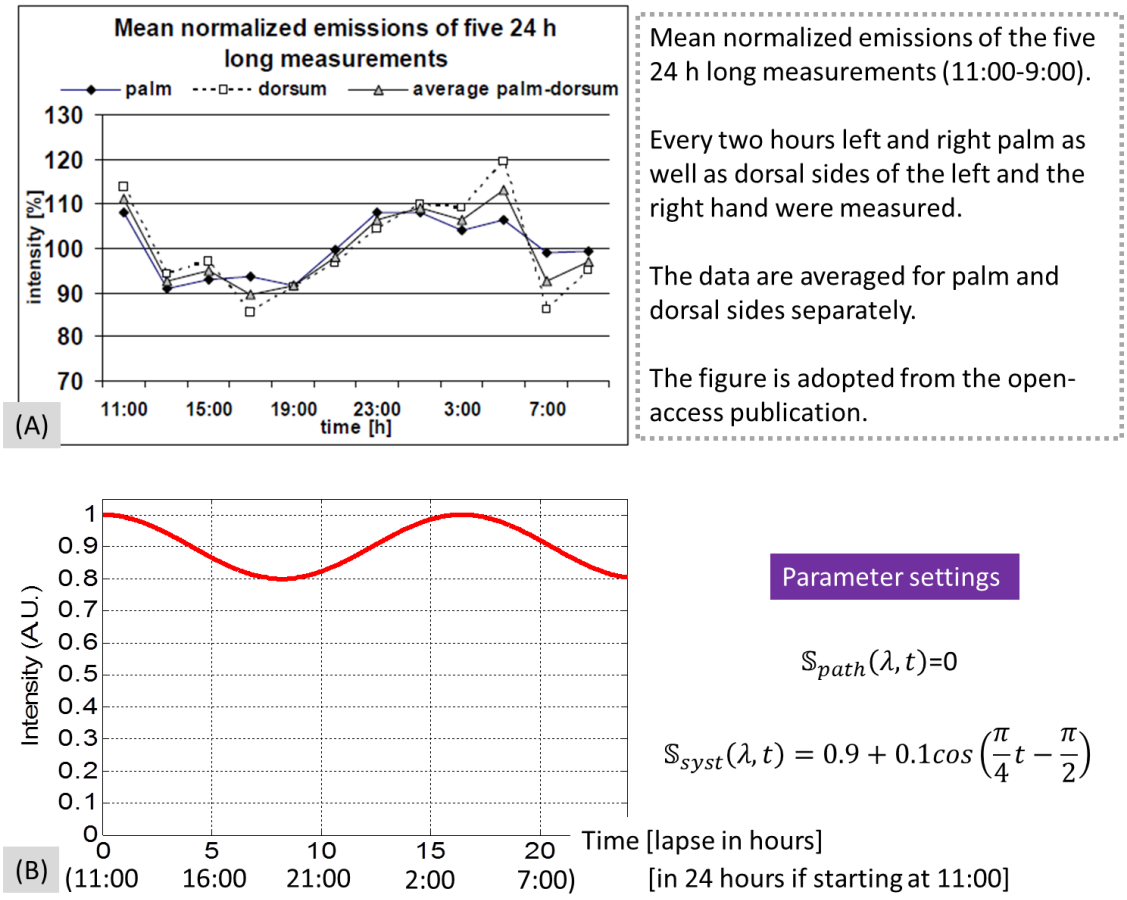


Figure 6. A literature report showing the diurnal variation of biophoton count is adopted from an open-access publication (CIFRA M, 2007) as shown in (A). The biophoton emission intensity revealed a trough at in later afternoon and a peak in early morning. That diurnal variation over a range of approximately 90-110% of the mid-line level can be directly associated with the circadian cycle. The variation of the photon fluence rate revealed at the boundary of the spherical tissue domain as a function of short-term homeostatic changes is simulated by removing $\mathbb{S}_{path}$ and setting the $\mathbb{S}_{syst}$ to change periodically. The circadian cycle is implemented into the intensity of physiological photo-genic source in Eq. (21) by setting $\mathbb{S}_{syst}(\lambda, t) = 0.9 + 0.1cos\left(\frac{\pi}{4}t - \frac{\pi}{2}\right)$.

Preprints (www.preprints.org) | NOT PEER-REVIEWED | Posted: 14 January 2019 doi:10.20944/preprints201810.0458.v2

### 4.3. Presentation of the spatial asymmetry associated with an asymmetric pathological condition

The spatial asymmetry of surface photon fluence rate can be induced by placing a pathological photo-genic source off-center in the spherical domain. Such a possibility is given in **Figure 7** in referencing the asymmetric spontaneous biophoton emission intensity that became aggregated as the tumor-load at the right axillary of a breast cancer mouse model increased (reproduced with permission from the publisher) (Zhao et al., 2017). The tumor volume is modeled as increasing exponentially (Jiang et al., 2011). The tumor volumes of respectively less than 0.5cm in diameter, between 1cm and 1.5cm in diameter, and greater than 1.5m in diameter as specified on panel (A) are modeled as $\exp(\frac{1}{1.5})$, $\exp(\frac{2}{1.5})$, and $\exp(\frac{3}{1.5})$ as plotted on the panel (B). The resulted numerical value of the tumor size is scaled down to 1% and used as the intensity of the pathological photo-genic source $\mathbb{S}_{path}$ that is placed at 1cm off the center at the right-lateral aspect and 1cm off center at the right anterior aspect, as illustrated in the left column of panel (C). In comparison, the centered physiological photo-genic source $\mathbb{S}_{syst}$ is set to have an intensity of 1. The intensity ratios of the centered physiological photo-genic source $\mathbb{S}_{syst}$ over the slightly off-centered pathological photo-genic source $\mathbb{S}_{path}$ for the three sizes of the tumor load are thus respectively 1 vs 0.0195, 1 vs 0.0379, and 1 vs 0.739. The resulted photon fluence rate over the surface of the spherical tissue domain that is projected to the middle cross-section and surrounded by a thin strip of the space beyond the tissue boundary is presented in the middle column of panel (C). The left-right asymmetry of the surface photon fluence rate becomes pronounced as the localized pathological photo-genic source increases in intensity. The 1-dimentional profile along the diameter crossing the 9 o'clock position to the 3 o'clock position of the 2-dimensional photon fluence rate map of the middle column of panel (C) is given at the right column. For a baseline arbitrary photon fluence rate of 300 over the tissue domain that is least affected by the pathological photo-genic source, the global change of the maximal photon fluence rate in the right lateral region of the side of the pathological photo-genic source increases from the baseline level to approximately 600. The pattern of the photon fluence rate at the right lateral side is similar to that of the literature pattern of spontaneous biophoton emission shown on panel (A). Meanwhile, the maximal photon fluence rate in the contra-lateral aspect of the pathological photo-genic source has increased slightly from the baseline, as the left-right difference becomes pronounced. This pattern of slight change of the contra-lateral normal side can also be traced back to the spontaneous biophoton emission pattern shown on panel (A).

Preprints (www.preprints.org) | NOT PEER-REVIEWED | Posted: 14 January 2019 doi:10.20944/preprints201810.0458.v2

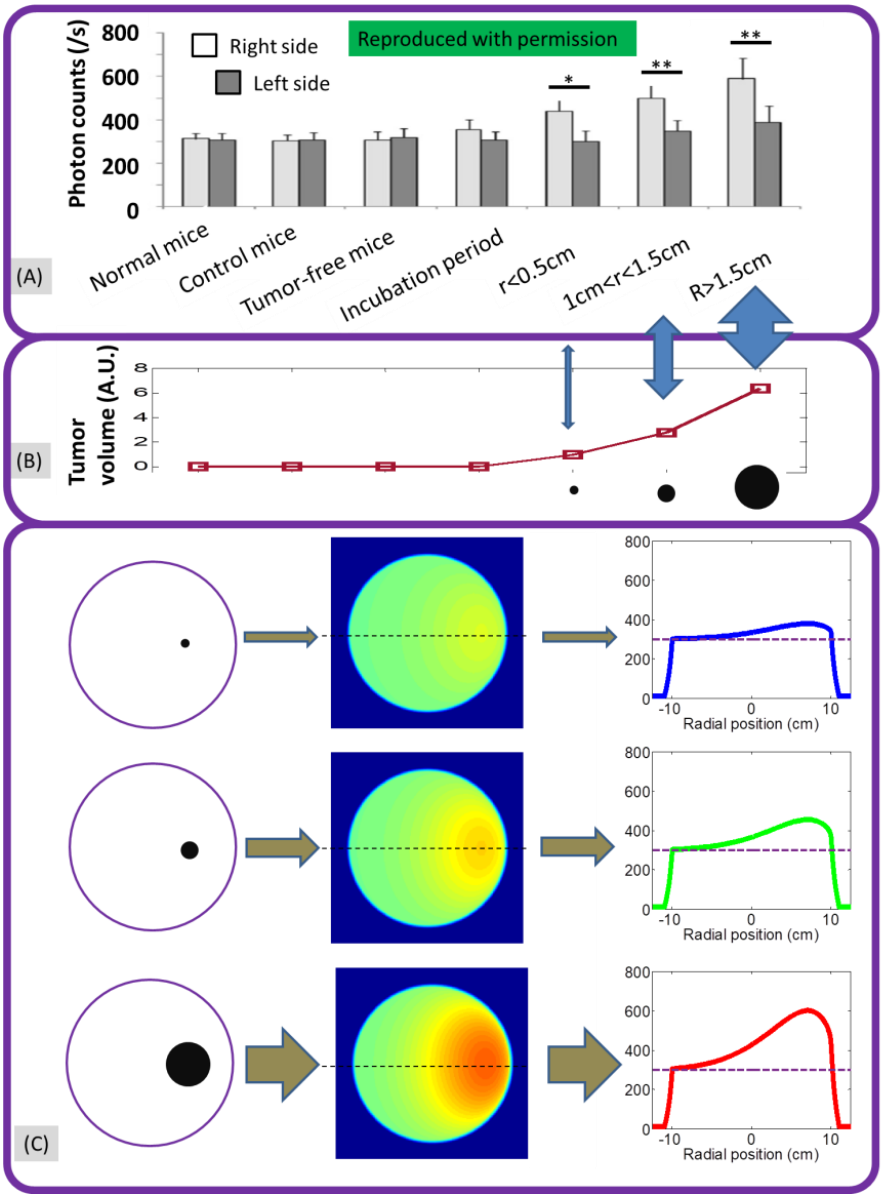


Figure 7. (A) the asymmetric biophoton emission intensity that became aggregated as the tumor-load at the right axillary of a breast cancer mouse model increased (Zhao et al., 2017). The tumor volumes of respectively less than 0.5cm in diameter, between 1cm and 1.5cm in diameter, and greater than 1.5m in diameter as specified on panel (A) are scaled as $\exp(\frac{1}{1.5})$, $\exp(\frac{2}{1.5})$, and $\exp(\frac{3}{1.5})$ as plotted on the panel (B). The resulted numerical value of the tumor size is scaled to 1% and used as the intensity of the pathological photo-genic source $\mathbb{S}_{path}$ that is placed at 1cm off the center at the right-lateral aspect and 1cm off center at the right anterior aspect, as illustrated in the left column of panel (C). The resulted photon fluence rate over the surface of the spherical tissue domain that is projected to the middle cross-section and surrounded by a thin strip of the space beyond the tissue boundary is presented in the middle column of panel (C). The 1-dimentional profile along the diameter crossing the 9 o'clock position to the 3 o'clock position of the 2-dimensional photon fluence rate map of the middle column of panel (C) is given at the right column.

Preprints (www.preprints.org) | NOT PEER-REVIEWED | Posted: 14 January 2019 doi:10.20944/preprints201810.0458.v2

## 5. Discussions

This work is intended to initiate a quantitative model-based interpretation of a few superficial patterns of steady-state spontaneous biophoton emission that are presented as associated with age, systematic physiology, and localized pathological conditions. An obvious limitation of the proposed model is influenced by the many unsolved problems about the origin of biophoton emission. As a result, the proposed model only simulates the general life processes from a macro perspective in mind, by including birth, sexual maturity, aging, and possible significant pathological states of human being as the macroscopic factors influencing the origin of biophoton emission through oxidative stress pathway. In addition, the contribution of organs to oxidative stress is complex thus discourages the simple expression of its translation to the (single) source of biophoton emission, even though the model could serve as a starting intuitive platform that can be added with more complexity of the disease model in the context of photo-genesis. Another apparent limitation of this model is the arbitrary valuing of the photo-genetic factor for converting the hypothetical differential change of the vivo-nergy to a physical source of light emission. The photo-genetic factor may not be specified unless the hypothetical alternative state of the energy as "vivo-nergy" can be validated. Another limitation is the modeling of the human tissue volume as a translucent and homogeneous spherical domain, even though it may be more realistic than the more commonly treated semi-infinite tissue domain. The human tissue is also extremely heterogeneous concerning photon propagation. The advantage of the present spherical tissue domain is the involvement of only one boundary as the geometry involves essentially a radial dependency. A more practical geometry of representing human tissue volume in terms of photon propagation may be a cylindrical domain of finite-length within which the similar photon diffusion approach can be applied and the heterogeneity in tissue optical properties for photon propagation can be included. Applying the photon diffusion approach to a finite length cylindrical tissue domain will also require considering boundary at two orientations, one is along the radial dimension and the other is along the polar aspect. That treatment may reveal that the strips of photon emission at the cranial and caudal aspects of the human body differ from the strips of photon emission at the lateral aspects of the human body (Van Wijk et al., 2014). Treating heterogeneous tissue optical properties will incur considerably more complex treatment than is dealt with in this present work.

In this work, the physiological photo-genic source is hypothesized to locate at the center of the human tissue domain, concerning the systematic influence of any homeostatic causes. Additionally, the localization of the pathological photo-genic causes to only one off-center source is rather arbitrary. But the results associated with a single off-center pathological photo-genic source can be conveniently expanded to the case of having multiple pathological conditions that each demands an individual photo-genic source. In such cases, multiple pathological photo-genic sources of different intensities (and different temporal presentations) can be localized at different positions that potentially represent their site-specific anatomy, and the spatially resolved photon fluence rates resulted from those multiple pathological photo-genic sources can be combined in a linear format to inform the composite photon fluence rate at the surface, and perhaps in 3-dimension for tomography or topography. For a more complicated tissue geometry and tissue with heterogeneous optical properties, the computation of the surface photon fluence rate may be conducted by using numerical procedures such as finite-element methods (FEM) (Arridge et al., 2000) for solving photon propagation problems. Implementing numerical methods such as FEM may also allow addressing complicated pathological photon-genic causes that are better represented by the source modeled over a continuous tissue volume of arbitrary shapes or extents if they all contribute to the hypothetical photo-genesis through the oxidative stress process.

The pathological condition has been hypothetically linked in this model with neuronal control in deriving the photo-genic source term. A site of pathological condition that has lost the

Preprints (www.preprints.org) | NOT PEER-REVIEWED | Posted: 14 January 2019 doi:10.20944/preprints201810.0458.v2

neural control will lead to no change of the vivo-nergy, thus smaller or zero intensity of the photon-genic source. A smaller photo-genic source will result in smaller superficial photon fluence rate at the geometric side of the pathological condition, or equivalently higher superficial photon fluence rate at the contra-lateral side. This arrangement of the neuronal control will make the model output in consistent with the observation of lower spontaneous biophoton emission at the hand of hemiparesis when compared to the normal contra-lateral hand (Jung et al., 2003). The validity of the photo-genic effect of neuronal control for the superficial patterns of spontaneous biophoton emission is subject to experimental examinations.

The macroscopic-scale temporal changes of the superficial photon fluence rate have been estimated in this work for a single case of diurnal-like variation over a short 24-hours period. The approach is however applicable to modeling macroscopically presented temporal changes over a time scale much different from a day-long period. Evaluating if the temporal changes of the superficial photon fluence rate over a longer-than-day scale will represent the temporal changes of biophoton emission over the similar time scale is in need of the knowledge of how the homeostatic changes over the same time scale may alter the physiological photo-genic process. The methodological conveniences of estimating the macroscopic-scale superficial photon fluence rate, on the other hand, may facilitate modeling the microscopic-scale temporal pattern of biophoton emission under short and strong stimulation or stress. This will require treating the photon diffusion problem as a strictly temporal problem with fast time-responses, not the steady-state problem with slower temporal modulation of the photo-genic source as is simplified in this part of the work for superficial profiling of steady-state spontaneous biophoton emission. Works are ongoing, based on time-domain photon propagation in association with the overarching hypothesis of this work, regarding a model-based approach to the kinetics of delayed biophoton emission observed under external stimulation or stress (Chwirot, 1988, Hagens et al., 2008).

## 6. Conclusions

In conclusion, I have presented an analytical hypothesis for interpreting a few patterns of steady-state spontaneous biophoton emission of human, including the systematic dependency on age, the diurnal variation, and the geometric asymmetry associated with serious asymmetrical pathological conditions. The hypothesis has assumed an alternative state of energy of human, termed vivo-nergy, which is considered to be associated with only metabolically active organisms that are also under neuronal control. The hypothesis projects a decrease of the vivo-nergy in human during growth beyond puberty, with the rate of decrease dictated by a time-scale set by the sexual maturity. The hypothesis also projects a modification of the vivo-nergy by the phases of systematic or homeostatic physiology. The hypothesis further postulates that the deviation of the physiology-modified vivo-nergy from the pre-puberty level is deteriorated by acquired organ-specific pathological conditions. A temporal differential change of vivo-nergy is hypothesized to proportionally cause oxidative stress that has known to be the physical source of biophoton emission. The human geometry is simplified as a homogeneous spherical domain. The resulted steady-state diffusion of the photon emitted from a photo-genic source in a human geometry is modeled by steady-state photon diffusion incorporating an extrapolated zero-boundary condition. The physiological photo-genic source is centered, and its intensity is determined by the age and systematic physiology combined. Comparatively, an acquired asymmetric pathology sets both the intensity and the off-center position of the pathological photo-genic source. When the photo-genetic sources are implemented in the photon diffusion model, the steady-state photon fluence rate at the surface of the simplified human-representing spherical domain resembles the superficially presented patterns of age-dependency, homeostatic variation, and pathology-induced asymmetry of spontaneous biophoton emission reported in experimental studies. The analytical method has the potential to

be extended towards time-domain analysis, for interpreting the delayed-illumination kinetics of biophoton emission under stimulation.

## References


ARRIDGE, S. R., DEHGHANI, H., SCHWEIGER, M. & OKADA, E. 2000. The finite element model for the propagation of light in scattering media: a direct method for domains with nonscattering regions. *Med Phys,* 27**,** 252-64.

BOVERIS, A., CADENAS, E., REITER, R., FILIPKOWSKI, M., NAKASE, Y. & CHANCE, B. 1980. Organ chemiluminescence: noninvasive assay for oxidative radical reactions. *Proc Natl Acad Sci U S A,* 77**,** 347-51.

BOVERIS, A., PUNTARULO, S. A., ROY, A. H. & SANCHEZ, R. A. 1984. Spontaneous Chemiluminescence of Soybean Embryonic Axes during Imbibition. *Plant Physiol,* 76**,** 447-51.

BURGOS, R. C., CERVINKOVA, K., VAN DER LAAN, T., RAMAUTAR, R., VAN WIJK, E. P., CIFRA, M., KOVAL, S., BERGER, R., HANKEMEIER, T. & VAN DER GREEF, J. 2016. Tracking biochemical changes correlated with ultra-weak photon emission using metabolomics. *J Photochem Photobiol B,* 163**,** 237-45.

CADENAS, E. 1984. Biological chemiluminescence. *Photochem Photobiol,* 40**,** 823-30.

CADENAS, E., ARAD, I. D., BOVERIS, A., FISHER, A. B. & CHANCE, B. 1980a. Partial spectral analysis of the hydroperoxide-induced chemiluminescence of the perfused lung. *FEBS Lett,* 111**,** 413-8.

CADENAS, E., BOVERIS, A. & CHANCE, B. 1980b. Low-level chemiluminescence of bovine heart submitochondrial particles. *Biochem J,* 186**,** 659-67.

CHWIROT, W. B. 1988. Ultraweak photon emission and anther meiotic cycle in Larix europaea (experimental investigation of Nagl and Popp's electromagnetic model of differentiation). *Experientia,* 44**,** 594-9.

CIFRA, M. & POSPISIL, P. 2014. Ultra-weak photon emission from biological samples: definition, mechanisms, properties, detection and applications. *J Photochem Photobiol B,* 139**,** 2-10.

CIFRA M, V. W. E., KOCH H, BOSMAN S, VAN WIJK R. 2007. Spontaneous Ultra-Weak Photon Emission from Human Hands Is Time Dependent. *RADIOENGINEERING,* 16**,** 15-19.

COHEN, S. & POPP, F. A. 1997. Biophoton emission of the human body. *J Photochem Photobiol B,* 40**,** 187-9.

COHEN, S. & POPP, F. A. 2003. Biophoton emission of human body. *Indian J Exp Biol,* 41**,** 440-5.

CONTINI, D., MARTELLI, F. & ZACCANTI, G. 1997. Photon migration through a turbid slab described by a model based on diffusion approximation. I. Theory. *Appl Opt,* 36**,** 4587-99.

DEVARAJ, B., USA, M. & INABA, H. 1997. Biophotons: Ultraweak light emission from living systems. *Current Opinion in Solid State & Materials Science,* 2**,** 188-193.

FEDOROVA, G. F., TROFIMOV, A. V., VASIL'EV, R. F. & VEPRINTSEV, T. L. 2007. Peroxy-radical-mediated chemiluminescence: mechanistic diversity and fundamentals for antioxidant assay. *Arkivoc***,** 163-215.

GALLAS, J. M. & EISNER, M. 1987. Fluorescence of Melanin Dependence Upon Excitation Wavelength and Concentration. *Photochemistry and Photobiology,* 45**,** 595-600.

HAGENS, R., KHABIRI, F., SCHREINER, V., WENCK, H., WITTERN, K. P., DUCHSTEIN, H. J. & MEI, W. 2008. Non-invasive monitoring of oxidative skin stress by ultraweak photon emission measurement. II: biological validation on ultraviolet A-stressed skin. *Skin Res Technol,* 14**,** 112-20.

HASKELL, R. C., SVAASAND, L. O., TSAY, T. T., FENG, T. C., MCADAMS, M. S. & TROMBERG, B. J. 1994. Boundary conditions for the diffusion equation in radiative transfer. *J Opt Soc Am A Opt Image Sci Vis,* 11**,** 2727-41.

HAVAUX, M., TRIANTAPHYLIDES, C. & GENTY, B. 2006. Autoluminescence imaging: a non-invasive tool for mapping oxidative stress. *Trends Plant Sci,* 11**,** 480-4.

HE, M., SUN, M., VAN WIJK, E., VAN WIETMARSCHEN, H., VAN WIJK, R., WANG, Z., WANG, M., HANKEMEIER, T. & VAN DER GREEF, J. 2016. A Chinese literature overview on ultra-weak photon emission as promising technology for studying system-based diagnostics. *Complement Ther Med,* 25**,** 20-6.

ISHIMARU, A. 1989. Diffusion of light in turbid material. *Appl Opt,* 28**,** 2210-5.

IVES, J. A., VAN WIJK, E. P., BAT, N., CRAWFORD, C., WALTER, A., JONAS, W. B., VAN WIJK, R. & VAN DER GREEF, J. 2014. Ultraweak photon emission as a non-invasive health assessment: a systematic review. *PLoS One,* 9**,** e87401.

JIANG, Z., PIAO, D., BARTELS, K. E., HOLYOAK, G. R., RITCHEY, J. W., OWNBY, C. L., ROCK, K. & SLOBODOV, G. 2011. Transrectal ultrasound-integrated spectral optical tomography of hypoxic progression of a regressing tumor in a canine prostate. *Technol Cancer Res Treat,* 10**,** 519-31.

JOEY M. CASWELL, B. T. D., MICHAEL A. PERSINGER 2014. Cerebral Biophoton Emission as a Potential

Factor in Non-Local Human-Machine Interaction. *Neuroquantology,* 12**,** 1-11.

JUNG, H. H., WOO, W. M., YANG, J. M., CHOI, C., LEE, J., YOON, G., YANG, J. S., LEE, S. & SOH, K. S. 2003. Left-right asymmetry of biophoton emission from hemiparesis patients. *Indian J Exp Biol,* 41**,** 452-6.

JUNG, H. H., YANG, J. M., WOO, W. M., CHOI, C., YANG, J. S. & SOH, K. S. 2005. Year-long biophoton measurements: normalized frequency count analysis and seasonal dependency. *J Photochem Photobiol B,* 78**,** 149-54.

KALAJI, H. M., GOLTSEV, V., BOSA, K., ALLAKHVERDIEV, S. I., STRASSER, R. J. & GOVINDJEE 2012. Experimental in vivo measurements of light emission in plants: a perspective dedicated to David Walker. *Photosynthesis Research,* 114**,** 69-96.

KAYATZ, P., THUMANN, G., LUTHER, T. T., JORDAN, J. F., BARTZ-SCHMIDT, K. U., ESSER, P. J. & SCHRAERMEYER, U. 2001. Oxidation causes melanin fluorescence. *Invest Ophthalmol Vis Sci,* 42**,** 241-6.

KOBAYASHI, M., IWASA, T. & TADA, M. 2016. Polychromatic spectral pattern analysis of ultra-weak photon emissions from a human body. *J Photochem Photobiol B,* 159**,** 186-90.

KOBAYASHI, M., KIKUCHI, D. & OKAMURA, H. 2009. Imaging of ultraweak spontaneous photon emission from human body displaying diurnal rhythm. *PLoS One,* 4**,** e6256.

MORAES, T. A., BARLOW, P. W., KLINGELE, E. & GALLEP, C. M. 2012. Spontaneous ultra-weak light emissions from wheat seedlings are rhythmic and synchronized with the time profile of the local gravimetric tide. *Naturwissenschaften,* 99**,** 465-72.

NAKAMURA, K. & HIRAMATSU, M. 2005. Ultra-weak photon emission from human hand: influence of temperature and oxygen concentration on emission. *J Photochem Photobiol B,* 80**,** 156-60.

OU-YANG, H. 2014. The application of ultra-weak photon emission in dermatology. *J Photochem Photobiol B,* 139**,** 63-70.

PEDERZOLI, L., GIROLDINI, W., PRATI, E. & TRESSOLDI, P. 2017. The Physics of Mind-Matter Interaction at a Distance. *Neuroquantology,* 15**,** 114-119.

PIAO, D., BARBOUR, R. L., GRABER, H. L. & LEE, D. C. 2015. On the geometry dependence of differential pathlength factor for near-infrared spectroscopy. I. Steady-state with homogeneous medium. *J Biomed Opt,* 20**,** 105005.

QUICKENDEN, T. I. & QUE HEE, S. S. 1974. Weak luminescence from the yeast Saccharomyces cerevisiae and the existence of mitogenetic radiation. *Biochem Biophys Res Commun,* 60**,** 764-70.

RAHNAMA, M., TUSZYNSKI, J. A., BOKKON, I., CIFRA, M., SARDAR, P. & SALARI, V. 2011. Emission of mitochondrial biophotons and their effect on electrical activity of membrane via microtubules. *J Integr Neurosci,* 10**,** 65-88.

REDDY, J. S. K. 2016. Could 'Biophoton Emission' be the Reason for Mechanical Malfunctioning at the Moment of Death? *Neuroquantology,* 14**,** 806-809.

SAUERMANN, G., MEI, W. P., HOPPE, U. & STAB, F. 1999. Ultraweak photon emission of human skin in vivo: influence of topically applied antioxidants on human skin. *Methods Enzymol,* 300**,** 419-28.

SLAWINSKI, J., EZZAHIR, A., GODLEWSKI, M., KWIECINSKA, T., RAJFUR, Z., SITKO, D. & WIERZUCHOWSKA, D. 1992. Stress-induced photon emission from perturbed organisms. *Experientia,* 48**,** 1041-58.

ST‐PIERRE, M. A. P. A. L. S. 2011. The Biophysics at Death: Three Hypotheses With Potential Application to Paranormal Phenomena. *Neuroquantology,* 9**,** 36-40.

SUN, M., VAN WIJK, E., KOVAL, S., VAN WIJK, R., HE, M., WANG, M., HANKEMEIER, T. & VAN DER GREEF, J. 2017. Measuring ultra-weak photon emission as a non-invasive diagnostic tool for detecting early-stage type 2 diabetes: A step toward personalized medicine. *J Photochem Photobiol B,* 166**,** 86-93.

VAN WIJK, R., VAN WIJK, E. P., VAN WIETMARSCHEN, H. A. & VAN DER GREEF, J. 2014. Towards whole-body ultra-weak photon counting and imaging with a focus on human beings: a review. *J Photochem Photobiol B,* 139**,** 39-46.

WANG, J. & YU, Y. 2009. Relationship between ultra-weak bioluminescence and vigour or irradiation dose of irradiated wheat. *Luminescence,* 24**,** 209-12.

WANG, Z., WANG, N., LI, Z., XIAO, F. & DAI, J. 2016. Human high intelligence is involved in spectral redshift of biophotonic activities in the brain. *Proc Natl Acad Sci U S A,* 113**,** 8753-8.

YANG W, Z. W., LV Y, ET AL. 1995. Ultraweak photon emission experimental study on the torso meridian of 80 healthy people. *Shenzhen Zhongxiyi Jiehe Zazhi,* 5**,** 1-3.

 doi:10.20944/preprints201810.0458.v2

YANG W, Z. W., SONG W, ET AL. 1996. Ultraweak photon emission experimentalstudy on the four limbs meridian of 130 healthy people. *Shanghai ZhenjiuZazhi.,* 15**,** 34-35.

ZHANG, A., PIAO, D., BUNTING, C. F. & POGUE, B. W. 2010. Photon diffusion in a homogeneous medium bounded externally or internally by an infinitely long circular cylindrical applicator. I. Steady-state theory. *J Opt Soc Am A Opt Image Sci Vis,* 27**,** 648-62.

ZHAO, X., PANG, J., FU, J., WANG, Y., YANG, M., LIU, Y., FAN, H., ZHANG, L. & HAN, J. 2017. Spontaneous photon emission: A promising non-invasive diagnostic tool for breast cancer. *J Photochem Photobiol B,* 166**,** 232-238.

ZHAO, X., VAN WIJK, E., YAN, Y., VAN WIJK, R., YANG, H., ZHANG, Y. & WANG, J. 2016. Ultra-weak photon emission of hands in aging prediction. *J Photochem Photobiol B,* 162**,** 529-534.

ZHENG R, L. J., LIN Y ET AL. 1983. The studies of the relationship between human body surface ultraweak luminescence and certain physiological state. *Shanghai Zhongyiyao Zazhi,* 1**,** 44-47.